Final Technical Report

N00014-16-1-2425
Localization Grid for Accurate Positioning Onboard a Carrier

Submitted by

Yimin D. Zhang, Ph.D., PI
Department of Electrical and Computer Engineering
Temple University, Philadelphia, PA 19122

To

Kenneth P. Iwanski, Ph.D.
Office of Naval Research
Code 35, Naval Air Warfare & Weapons
875 N. Randolph St.
Arlington, VA 22203

Contributors

Dr. Yimin Zhang
Mr. Eric Pauls

June 2017

List of Contents

Executive Summary

This final report presents the results of the research and development performed under ONR grant number N00014-16-1-2425 over the period of June 1, 2016 to May 31, 2017. The research team working on this project consists of Prof. Yimin Zhang (PI) and Mr. Eric Pauls (Graduate student at Villanova University; currently with Harris Corporation).

We have also collaborated with the team of the Robotics and Intelligent Systems Engineering (RISE) Lab at NAVAIR Lakehurst, New Jersey, consisting of Mr. Larry Venetsky, Mr. Christian Ramos, Dr. James Hing, Mr. Kyle Hart, and Dr. Christopher Thajudeen. We provided technical supports for the RISE Lab to perform experimental verification to assess the feasibility of the techniques we have developed in this project.

The objective of this project is to develop implementable solutions that achieve the required instantaneous position and orientation tracking accuracy of aircrafts onboard a deck with the radio frequency identification (RFID) technologies. RFID tags covering the entire flight deck and hanger bay areas serve as anchors with known locations, whereas an aircraft, through multiple RFID reader antennas which are fixed on the aircraft, senses the relative position information with nearby RFID tags and determines its own instantaneous position and orientation.

The project contains the following three major technical tasks: 1. Development of tracking algorithms; 2. Proof-of-concept experiment verification; and 3. Region of interest identification via computer vision.

This project is the continuation of ONR contract N00014-14-C-0005, which was awarded to Villanova University for the period between February 14, 2014 and February 13, 2016. ONR contract N00014-14-C-0005 was terminated without full completion due to the PI's move from Villanova University to Temple University during the project. As such, for completeness and convenience, this report contains materials that overlap with the final report of ONR contract N00014-14-C-0005.

In the following, we report the results of the conducted research and development in the abovementioned three major tasks.

1. Development of Tracking Algorithms

1.1. Introduction

A typical RFID system consists of RFID readers, reader antennas, and RFID tags. The reader "polls" for present tags by radiating electromagnetic waves through the reader antenna. Tags, which consist of a compact integrated circuit and antenna supported by an application-specific body, receive some of the transmitted waves and send back their unique identifying code by means of backscattering. There are several variations of tag types to fit specific applications and transmission regulations. In this work, we employ passive ultra-high frequency (UHF) tags. These tags are popular for localization solutions as they require no power supply other than radiation from the reader, and can operate reliably for a range of up to a few meters.

Localization through RFID is achieved by using an RFID system to sense a certain reader-tag arrangement and then deducing position information from this measurement. We achieve RFID

localization based on the signal strength of the backscattered radiation, referred to as the received signal strength indicator (RSSI), which is related to the distance between the reader and the tag, and their orientations. As such, RSSI metrics measured at the reader corresponding to multiple nearby tags allow reader localization, with respect to the tags, through maximum likelihood (ML) estimation. Tracking of aircraft location and orientation is achieved using multiple RFID readers from their instantaneous locations.

1.2. RSSI-based Localization

RSSI is a measure of the received power of a radio transmission that is related to the ratio of the received power from a responding tag to the transmitted power from the RFID reader. Signal power in a two-way line-of-sight RFID transmission as a function of distance can be modeled using the Friis transmission equation, expressed as

$$P_{\mathrm{Rx}} = P_{\mathrm{Tx}} G_{\mathrm{tag}}^2 G_{\mathrm{read}}^2 \left(\frac{\lambda}{4\pi d}\right)^4, \tag{1.1}$$

where P_{Rx} and P_{Tx} are the received and the transmitted power at the reader antenna, G_{tag} and G_{read} are the gains of the tag and reader antennas, d is the distance between the reader antenna and the tag, and λ is the wavelength of the signal. For the UHF RFID system being used, the carrier frequency is bounded in the 902–928 MHz range, so the corresponding wavelength varies between 0.323 meter and 0.333 meter (mean value 0.328 meter).

To improve the accuracy of the transmission equation, the gain of the reader antenna and the tag antenna can be expressed as functions of direction angles, and the power efficiency of the tag can be expressed as a constant η, which is typically about 1/3 [1, p. 77]. That is,

$$P_{\mathrm{Rx}} = P_{\mathrm{Tx}} \eta G_{\mathrm{tag}}^2(\theta_{\mathrm{tag}}) G_{\mathrm{read}}^2(\theta_{\mathrm{read}}) \left(\frac{\lambda}{4\pi d}\right)^4. \tag{1.2}$$

In the effective reading range of an RFID reader/antenna system operating at the limit transmission power allowed by the United States Federal Communications Commission (FCC), which is 4 Watts or 36 dBm, the transmit/receive power ratio is expected to be between -10dBm and -100 dBm [1]. As there is no standard for RSSI measurements, manufacturers of RFID readers can choose to report RSSI on an arbitrary scale. The actual RSSI value reported from a reader may be heavily manipulated from the original power ratio. For example, in the Alien ALR-9680 RFID reader model used in this work, the RSSI is mapped to a linear scale with respect to the range. In practical applications of RSSI-based localization, it is important to understand the relationship between the reader's RSSI value and the true power measurement P_{Rx}.

With an accurate model for RSSI as a function of position, it is possible to combine RSSI measurements from multiple tags to localize an RFID reader. In this paper, we explore the process of generating an RSSI model, which is then applied to a localization problem to precisely estimate the position of a reader in a field of tags.

1.3. RSSI Model from Experiments

To understand and characterize the performance of RFID systems and to achieve accurate RSSI measurements, we conducted experiments using an RFID reader and RFID tags to examine the

RSSI metric in terms of the tag performance, manufacturing differences between tags, and changes in RSSI with different positions and orientations of the tags. Experimental studies on the variation in performance across different tags, the measurement error associated with each RSSI recorded, and the effects of tag mounting surfaces on RSSI reveal several potential sources of error in RSSI-based RFID localization. In this section, we present experimental results of RSSI measurements, and discuss possible sources of RSSI errors and remedy solutions. Note the RSSI model established from each experiment is only valid for the specific setting.

We first examine the RSSI model in the absence of ground reflections. The effect of metal floor, as expected in deck operation, will be examined later.

1.3.1. Experimental Setting

The reader setup for the experiments includes an Alien ALR-9680 RFID reader with transmit power of 1W (30 dBm) communicating in the UHF frequency band between 902.75-927.25 MHz. The reader is connected to a Poynting Patch-A0026 right hand circularly polarized antenna with a nominal gain of 6.5dBi (±0.5dB) and 3dB beamwidth of 60° (±5°) and 74° (±5°) in elevation and azimuth, respectively. Alien Squiggle Higgs3 passive UHF RFID tags are used for the experiments. As shown in Fig. 1.1, the experiments were performed on a wooden frame designed to hold the antenna and tags in specific locations in space while minimizing electromagnetic reflections. Additionally, electromagnetic absorbing mats were placed on the floor beneath the test setup to eliminate reflections from the laboratory floor.

Figure 1.1. Wooden frame holding reader, antenna, and RFID tags above a floor of electromagnetic absorbers.

1.3.2. Tag RSSI Performance

We first perform an experiment on tags at a fixed position to observe the variation in RSSI measurements over 500 repeated reads. The measurement data for a single tag at a distance of 76

cm (20 inches) is shown in Fig. 1.2 for the first 100 reads. It is clear that the RSSI measurement varies significantly over the different reads. It should also be noted that, for the specific RFID reader being used, the RSSI measurements are quantized by the reader to integer values with no measurement unit.

The experiment was then repeated with 45 tags at 500 reads each to study the differences in RSSI performance between different tags, and the results are shown in Fig. 1.3. It is observed from Fig. 3(a) that all of the 45 tags tested show very similar standard deviation of about 1.57. The mean RSSI for each tag, however, varies significantly in this experiment. Fig. 1.3(b) shows the histogram of the mean RSSI for the 45 tags, which clearly demonstrate that the same type of tags from the same manufacturer can still perform differently. Therefore, to effectively account for both the variation in RSSI measurements for a specific tag and the variation in performance between different tags, the tags should be "pre-screened" to select only tags that perform similarly when tested in the same setting. For this experiment, we chose tags within the 92-92.25 RSSI range at a distance of 30 inches. With a set of similarly performing tags selected, the number of tag reads to average together can be chosen to achieve a desired accuracy of the mean RSSI.

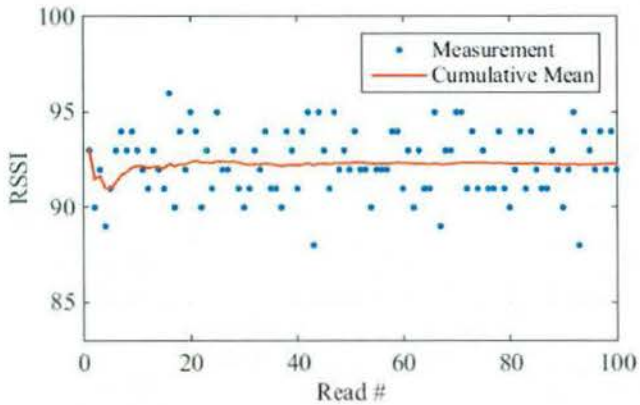

Figure 1.2. Variations in RSSI readings for a single fixed tag.

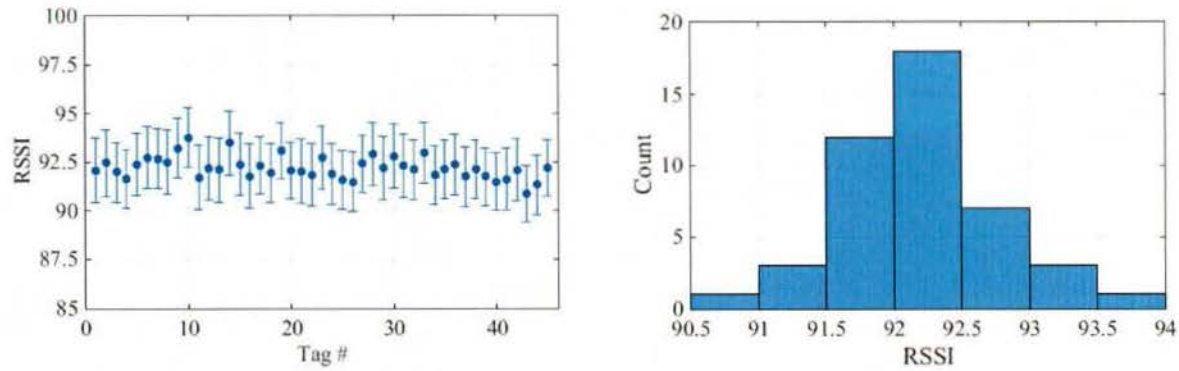

(a) (b)

Figure 1.3. RSSI measurements over 45 tags (500 measurements per tag). (a) error-bar plot with mean and standard deviation; (b) histogram.

Fig. 1.4 shows an example of the cumulative progression of mean RSSI for 4 tags as the number of tag reads increases. The RSSI for each tag converges to within ±0.25 of the final mean in about 37 samples. The averaged RSSI converges approximately after 15 reads with a standard deviation of 1.65. Recording RSSI as the mean value of several measurements helps to eliminate both measurement noise and the quantization noise caused by the reader's integer rounding.

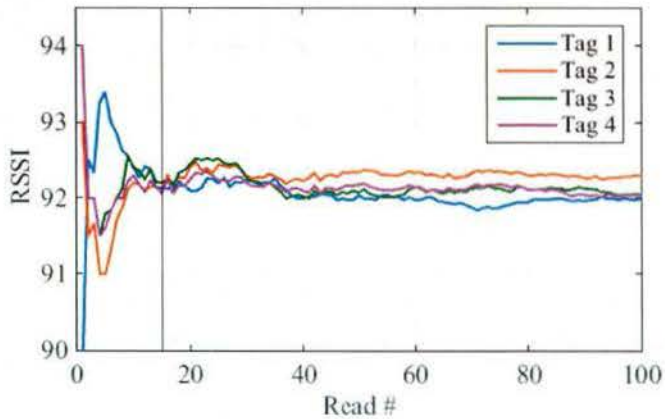

Figure 1.4. Progression of cumulative mean RSSI for 4 RFID tags.

1.3.3. RSSI versus Distance between RFID Reader and Tag

To study the relationship between the RSSI and the distance between the RFID reader and tag, we place an RFID tag underneath the RFID reader antenna with a varied distance. Fig. 1.5 shows the RSSI mean and standard deviation over 500 reads with the reader-tag distance varying from 30 cm (12 inches) to 1.94 m (76.5 inches).

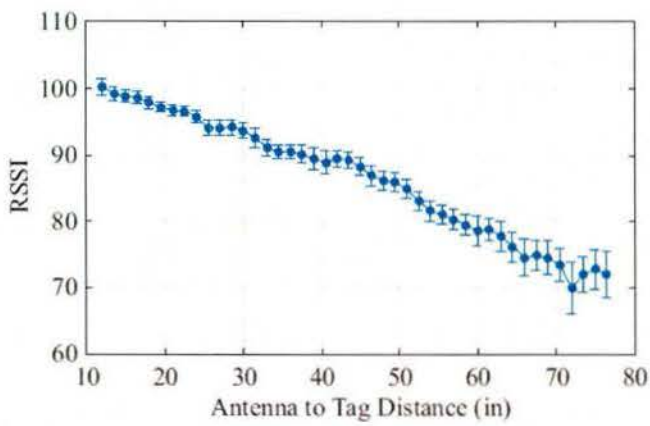

Figure 1.5. RSSI versus distance between reader antenna and tag.

This experiment shows that the reader's reported RSSI varies linearly with distance. Additionally, the standard deviation for RSSI measurements increases with distance. Small variations in the data can be attributed to small amounts of multipath interference from the test environment. It should

be noted that this linear relationship is caused by a linearization algorithm (discussed in Section 1.3.4) that is specific to the RFID reader.

1.3.4. RSSI versus Tag Orientation Angle

The Alien Squiggle tags, as well as many other commonly used RFID tags, are of a dipole design. Therefore, their transmission/receive strength can be expected to vary significantly with changes in angle. The gain decreases as the axis of the tag becomes more closely aligned with the line of sight to the reader because of the toroid-shaped radiation pattern of the tag. The angle θ (shown in Fig. 1.6(a)) is defined as the orientation angle of the tag relative to the reader-tag line of sight. For a given reader and tag setup, θ is calculated as

$$\theta = \cos^{-1}\left(\frac{\vec{a}\cdot\vec{b}}{\|\vec{a}\|\|\vec{b}\|}\right), \tag{1.3}$$

where $\vec{a}$ is the line of sight unit vector from the reader to the tag, and $\vec{b}$ is a unit vector in the direction of the tag's axis. To study the relationship between the RSSI and the orientation angle θ, we place an RFID tag beneath the RFID reader antenna at a fixed distance of 76 cm (30 inches) and rotate the tag such that θ increases in increments of 5°. The results of this experiment in Fig. 1.7 show that the orientation angle θ has a significant effect on the RSSI. Similar to an ideal dipole, the directive signal strength is sinusoidal and approximately symmetric about 0°. Accounting for the change in RSSI with respect to θ in the context of ML estimation allows for significant improvement over a traditional multilateration approach.

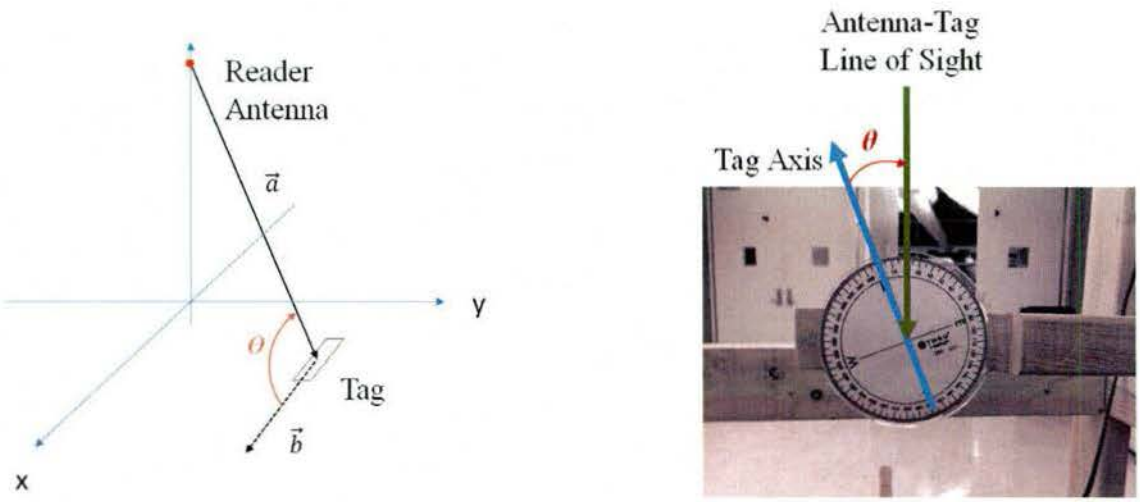

(a) (b)

Figure 1.6. (a) Depiction of θ, the three-dimensional angle between the tag antenna axis and the line of sight from the reader antenna to the tag. (b) Experiment setup for measuring RSSI while varying θ.

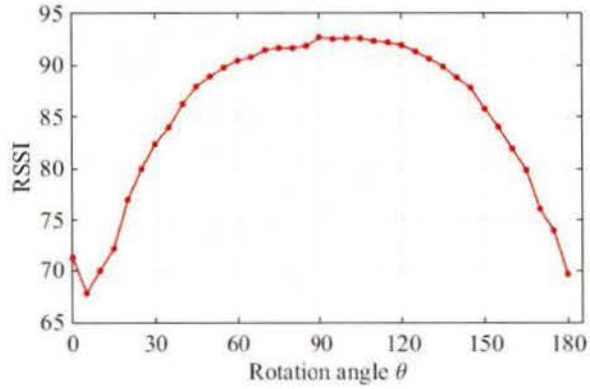

Figure 1.7. Average of 500 RSSI reads versus tag angle θ. 0° indicates that the tag axis is perpendicular to the line of sight to the reader antenna.

1.3.5. RSSI Transform Model

The data from Sections 1.3.2 and 1.3.3 allow us to create a model for RSSI as a function of orientation angle and distance in the form of Equation (1.2). We first account for the linearization performed by the RFID reader. We observe that RSSI reported from the reader varies linearly with distance, which is achieved by performing a transformation on the received signal power measurement

$$RSSI = F - \left(\frac{P_{Rx}}{P_{Tx}}\right)^{-1/4}. \tag{1.4}$$

By substituting the equation for received power P_{Rx} from (1.2), we derive the equation for mapping the RFID reader's RSSI measurement to signal power to be

$$RSSI(d,\theta) = F - \left(\frac{A \times G_{\mathrm{tag}}(\theta)}{d^4 + k}\right)^{-1/4}, \tag{1.5}$$

where F is an additive constant within the reader, k is a small constant to account for nonlinearities in the reader's measurements, and A is a scaling factor that encompasses the term $\left(\frac{\lambda}{4\pi}\right)^4$, tag loss η, and G_{read}, which is assumed to be constant within the main beam of the reader antenna. As the tag's directive gain is very close to that of an ideal dipole, we can model $G_{\mathrm{tag}}(\theta)$ as

$$G_{\mathrm{tag}}(\theta) \propto |(\sin(\theta - \varphi)|^b, \tag{1.6}$$

with phase adjustment φ and exponent b to account for the small differences between an ideal dipole and the Alien Squiggle inlay antenna. Equations (1.5) and (1.6) yield a complete characterization of RSSI with respect to distance and tag direction. By fitting equation (1.5) to the experimental data for distance and angle, we find the values for the RSSI equation constants as

$$RSSI(d,\theta) = F - \left(\frac{A \times |(\sin(\theta - \varphi)|^b}{d^4 + k}\right)^{-1/4}. \tag{1.7}$$

where the constants are summarized in Table 1.1.

Table 1.1. Estimated parameters for RSSI transform

F	A	k	φ	B
109	1.363×10^5	3.445×10^{-7}	5°	2.5

1.4. Reader Localization Algorithm and Experimental Validation

The search area to be considered is an N_x x N_y rectangular grid of possible locations for the reader. For a set of N_T tags, let $\mathbf{\Phi}$ be an $N_T \times N_x N_y$ dictionary matrix where the kth column of $\mathbf{\Phi}$ is expressed as

$$\mathbf{\Phi}_k = \left[\phi_1^k, \phi_2^k \ldots, \phi_{N_T}^k\right]^T, \; k = 1, \ldots, N_x N_y, \tag{1.8}$$

where $(.)^T$ denotes vector transpose. The element ϕ_i^k is the expected RSSI measurement at the kth hypothetical reader grid position (x_k, y_k, z_k) and the ith tag located at (x_i, y_i, z_i). The reader antenna is placed at a fixed height $z_k=h$, and all tags will be placed on the same reference plane with height $z_i=0$. In this case, the expected RSSI measurement table can be populated with $\phi_i^k = RSSI\left(d_i^k, \theta_i^k\right)$ given in Equation (1.6), where

$$d_i^k = \sqrt{(x_k - x_i) + (y_k - y_i) + h^2}\,, \tag{1.9}$$

and θ_i^k is calculated from Equation (1.3) as the angle between the tag axis and the tag-reader line of sight. With the expected RSSI matrix $\mathbf{\Phi}$ calculated, localization of the reader is performed by comparing an input RSSI measurement vector to the columns of $\mathbf{\Phi}$. The measurement vector $\mathbf{y}$ contains RSSI data for N_T tags averaged over a predetermined number of reads. The elements of $\mathbf{y}$ are arranged to correspond to the rows of $\mathbf{\Phi}$. Note that not all of the tags will successfully communicate with the reader during a reading attempt. Tags with no response should be removed from the RSSI measurement vector $\mathbf{y}$, and their corresponding rows of $\mathbf{\Phi}$. The kth column of $\mathbf{\Phi}$ is then found by solving [2]

$$\arg\min_k \|\mathbf{y} - \mathbf{\Phi}_k\|. \tag{1.10}$$

For large and/or very fine localization grids, computation time can be greatly reduced for real-time tracking applications by limiting k (and subsequently (x_k, y_k, z_k)) to positions within a certain radius of the previous localization estimate.

1.5. Reader Tracking Algorithm

For tracking the trajectory of the reader, we resort to the Kalman filter. We define the state vector of the reader at the τth observation as a four-dimensional (4-D) vector $\mathbf{x}_\tau = [\mathbf{q}_\tau^T, \mathbf{v}_\tau^T]^T$, comprising its position vector $\mathbf{q}_\tau = [q_x, q_y, q_z]^T$ and velocity vector $\mathbf{v}_\tau = [v_x, v_y, v_z]^T$ in the two-dimensional

(2-D) Cartesian coordinate system. The reader dynamics is assumed to evolve according to a constant velocity linear Gaussian model, such that

$$\mathbf{x}_\tau = \mathbf{F}\mathbf{x}_{\tau-1} + \mathbf{w}_\tau, \tag{1.11}$$

where $\mathbf{F}$ is the state transition matrix defining the linear dynamics, expressed as

$$\mathbf{F} = \begin{bmatrix} \mathbf{I}_2 & \Delta\mathbf{I}_2 \\ \mathbf{0}_2 & \mathbf{I}_2 \end{bmatrix}, \tag{1.12}$$

Δ is the sampling interval, and $\mathbf{w}_\tau$ is the process noise vector modeled as additive white Gaussian with zero mean and variance matrix $\mathbf{Q}$. The process noise covariance matrix can be expressed as

$$\mathbf{Q} = \sigma_w^2 \begin{bmatrix} \frac{\Delta^3}{3}\mathbf{I}_2 & \frac{\Delta^2}{2}\mathbf{I}_2 \\ \frac{\Delta^2}{2}\mathbf{I}_2 & \Delta\mathbf{I}_2 \end{bmatrix}. \tag{1.13}$$

For each observation instant τ, we feed the ML estimates of the instantaneous reader position as a measurement to the Kalman filter. We define the measurement vector as $\mathbf{z}_\tau = [\hat{\mathbf{q}}_\tau^T, \mathbf{v}_\tau^T]^T$, where $\hat{\mathbf{q}}_\tau^T$ is the ML estimate of the instantaneous reader position obtained from Equation (1.10). Since this is a self-localization problem, we assume the prior knowledge of the instantaneous velocity. As such, we can define the measurement vector as

$$\mathbf{z}_\tau = \mathbf{H}_\tau \mathbf{x}_\tau + \boldsymbol{\eta}_\tau, \tag{1.14}$$

where $\mathbf{H}_\tau = \mathbf{I}_4$ is the matrix mapping the measurement to the target state space and $\boldsymbol{\eta}_\tau$ is the measurement noise modeled as an additive white Gaussian vector with zero mean and covariance matrix $\mathbf{R}_\tau$. As such, following the conventional Kalman filter formulations [4], we obtain the predictions for the state vector and the corresponding covariance matrix, respectively, as

$$\hat{\mathbf{x}}_{\tau|\tau-1} = \mathbf{F}\hat{\mathbf{x}}_{\tau-1|\tau-1}, \tag{1.15}$$

and

$$\mathbf{P}_{\tau|\tau-1} = \mathbf{Q}_{\tau-1} + \mathbf{F}\mathbf{P}_{\tau-1|\tau-1}\mathbf{F}^T. \tag{1.16}$$

Likewise, the updates are obtained as

$$\hat{\mathbf{x}}_{\tau|\tau} = \hat{\mathbf{x}}_{\tau|\tau-1} + \mathbf{K}_\tau(\mathbf{z}_\tau - \mathbf{H}_\tau\hat{\mathbf{x}}_{\tau|\tau-1}), \tag{1.17}$$

and

$$\mathbf{P}_{\tau|\tau} = \mathbf{P}_{\tau|\tau-1} - \mathbf{K}_\tau\mathbf{S}_\tau\mathbf{K}_\tau^T, \tag{1.18}$$

where $\mathbf{S}_\tau$ is the covariance matrix of the innovation term $\mathbf{s}_\tau = \mathbf{z}_\tau - \mathbf{H}_\tau\hat{\mathbf{x}}_{\tau|\tau-1}$, and $\mathbf{K}_\tau = \mathbf{P}_{\tau|\tau-1}\mathbf{H}_\tau^T\mathbf{S}_\tau^{-1}$ represents the Kalman gain.

1.6. Software Development

We have developed prototype software to collect data from RFID readers and process the data for aircraft localization and tracking. The software is developed to operate in the Microsoft Windows platform. The main program is running in the MathWorks Matlab platform. When performing data collection, functions developed using Java is executed.

In this current phase, we have made several revisions of the software to achieve faster RFID tag reading, enable simultaneous data reading at multiple RFID readers and multiple RFID reader antennas, and improve the accuracy and robustness of the aircraft localization and tracking in impaired propagation environments.

1.7. Collaboration with and Support for NAVAIR RISE Lab

Throughout the entire project, we have closely collaborated with the NAVAIR RISE Lab. The RISE Lab has advised our development and experimental studies.

RISE Lab carried out experimental campaign between October 2014 and December 2016 in order to assess the feasibility of the techniques we have developed in this project. To support RISE Lab's efforts, we have provided the RISE Lab with the system recommendations and the required software. The software is based on the prototype we have developed for our own use, but has been modified with a more user-friendly interface.

Fig. 1.8 shows the expeimental scene at the RISE Lab.

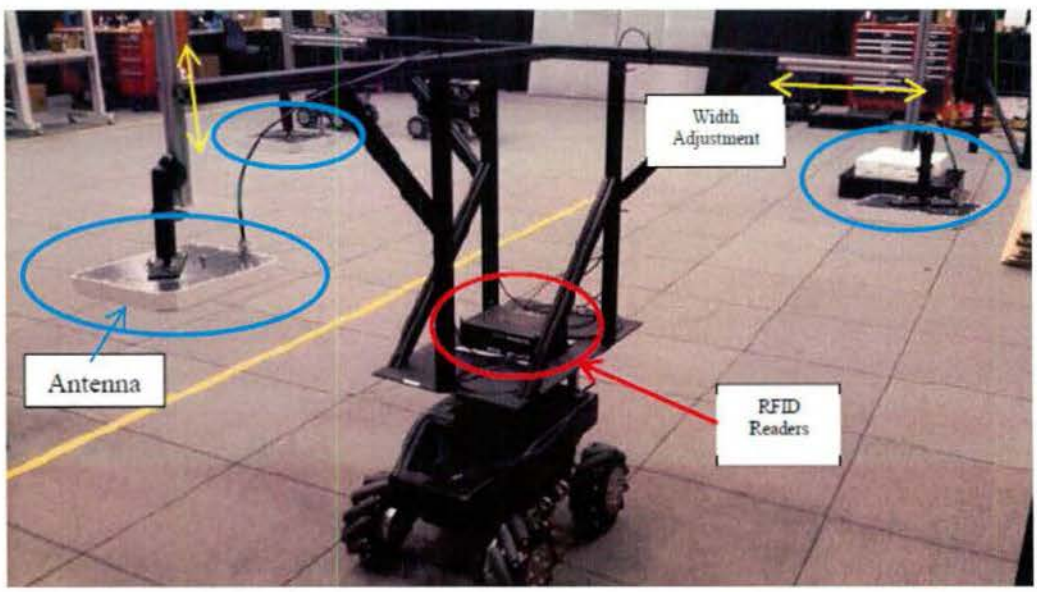

Figure 1.8. Experimental scene at the NAVAIR RISE Lab (photo provided by the RISE Lab).

2. Proof-of-Concept Experiment Verification

2.1. Set-Up of RFID Test Platform

We have set up an RFID test platform for reading passive tags. The test platform consists of a computer, an Alien ALR-9680 RFID reader, and a Poynting patch antenna (Fig. 2.1). The computer and the reader are connected with a router which supported both wired and wireless local area network (LAN) connections. Both standard inlay tags (see Fig. 2.1(c)) and metal surface tags (see Fig. 2.1(d)) are used in the experiments.

(a) Alien ALR-9680 RFID reader

(b) Poynting Patch-A0026 Linear Patch Antenna

(c) Alien Squiggle Higgs3 ALN-9640 general purpose passive UHF tag

(d) Omni-ID Max metal surface passive UHF tag

Figure 2.1. RFID reader, reader antenna, and tags.

In addition, we have built two wood tables, shown in Fig. 2.2, to mount the test platform with adjustable reader antenna height and tag positions. The tables enabled us to:

(a) Measure the RSSI with insignificant effect of ground and environment reflections. If needed, the effect of such reflections can be further reduced by properly placing electromagnetic absorbers;
(b) Emulate metallic or composite material reflections at different positions (e.g., on top of the table for wing reflection, and at the bottoms for ground reflection);
(c) Place RFID tags in multiple fixed turnable positions to measure the variation of RSSI for different tags and the effect of tag orientations;
(d) Move the table to measure tag RSSI in a dynamic environment.

Fig. 2.2. Two wood tables used in the experiment.

The reader communicates over a closed LAN with the computer through the router. The computer signals the reader to scan for tags and report the tag ID and the RSSI back. We have developed software to send control commands to the readers and receive data from the reader with the Telnet protocol, and store the received data to computer for offline processing.

2.2. Simulation Evaluation of Tag Radiation Pattern

In order to understand the characteristics of general purpose passive RFID tags in different environments, particularly the metallic deck surface, we have performed computer simulations using Computer Simulation Technology (CST) Microwave Studio prior to our experimental studies. In the following, we report the simulation model of the RFID tag, and the results of the scattering parameter S_{11} for RFID tags near a metallic plane. The S_{11} parameter describes the input port voltage reflection coefficient of the RFID tag and the value should be very small in the resonant frequency [5]. On the other hand, a high value of the S_{11} parameter implies ineffective radiation.

2.2.1. RFID Tag Placed on Metal

We use the Alien Squiggle passive UHF RFID tag for the analysis of the electromagnetic characteristics. The tag has a resonance frequency at 915 MHz with the expected radiation characteristics in the free space. The tag model is shown in Fig. 2.3, which is modeled in CST Microwave Studio. We place the tag at different heights above a conducting ground plane and then moved farther from the surface in 1 mm increments from 1 mm to 10 mm total height. The resulting S_{11} parameter values are plotted in Fig. 2.4. From Figure 2.4 it is observed that a good match is achieved when the distance is greater than 10 mm.

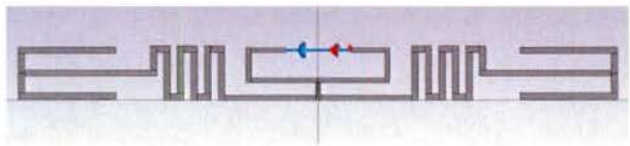

Figure 2.3. CST Microwave Studio geometry of Alien Squiggle tag.

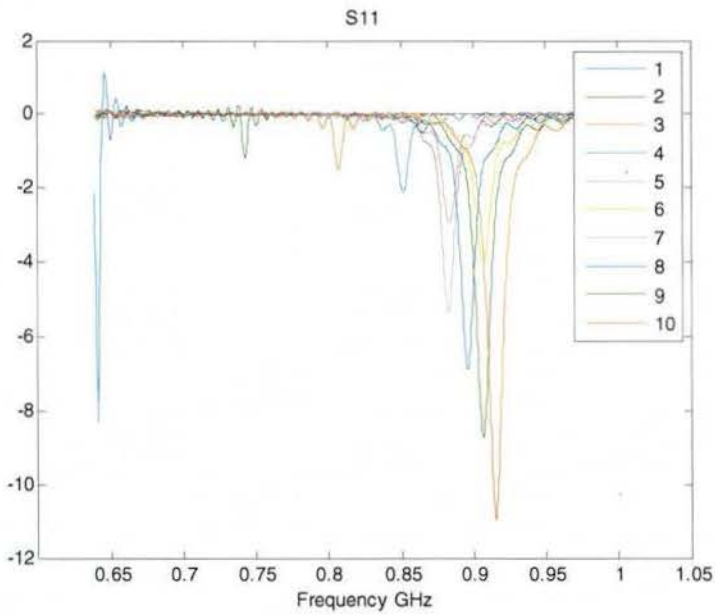

Figure 2.4. Simulated S_{11} parameter values of RFID tag at 1 mm to 10 mm above the metallic ground.

2.3. Measured RSSI of Standard Tags (Non-Metal Surface Tags)

2.3.1. Alien Tags on Building Floor and Metallic Surface

Section 1.3 reported some experimental results in a controlled environment where the surrounding reflections and scatterings are avoided by placing electromagnetic absorbers. To evaluate the RFID reading performance in a practical environment, we have conducted experiments with the electromagnetic absorbers removed, and the RSSI are measured on building floors and metallic floors.

To emulate metallic surface, as we reported in the last report, we have purchased four 36" x 36" aluminum 6061-T6 Bare Sheets (thickness 0.125") to be placed on the floor. RFID tags are placed on the floor or metallic surface, and the RSSI evaluation is made with different heights of air or dielectric cushion space between the RFID tag and the floor or metallic surface.

We first tested the case where Alien Squiggle RFID tags, which are not designed for use on metallic surface, are placed on the metallic surface using aluminum sheets. The experimental scene is shown in Figure 2.5(a). The vertical distance between the RFID tag and the reader antenna is 60" (1.52 m) and the horizontal distance is 17" (0.43 m). In this case, the RFID reader fails to read the RSSI result. This is expected from electromagnetic theory because the metallic surface generates a negative tag image that cancels the tag radiation, and the presence of the metallic surface also alters the resonant frequency of the tag.

The RSSI measurement for tags placed on the building floor was also unavailable. The vertical distance between the RFID tag and the reader antenna is 60" (1.52 m) and the horizontal distance is about 36" (0.91 m), as shown in Fig. 2.5(b).

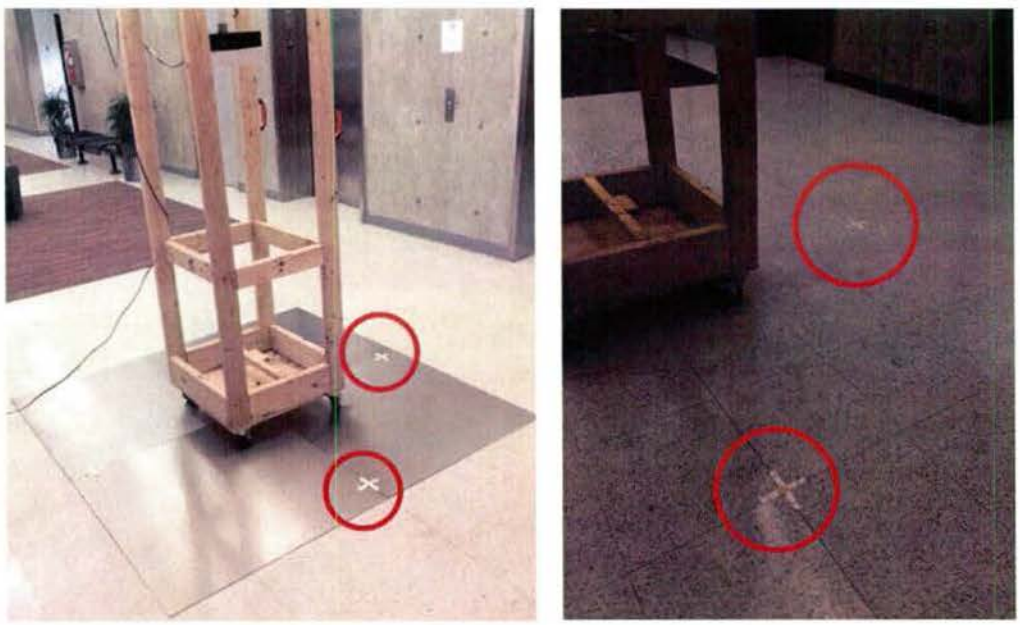

(a) Metallic surface (b) Building floor

Fig. 2.5. RFID tags placed on (a) metallic surface and (b) building floor.

2.3.2. Measured RSSI with Air Gap between Standard Tag and Metallic Sheet

As discussed in Section 2.2, placing the RFID tags above the metallic surface with certain height of air gap would reduce the effect of the metallic surface. In particular, it is suggested that a 10-mm air gap between the tag and the metallic surface would yield insignificant impact of the metallic surface to the tag resonant frequency.

To experimentally confirm this result, we have tested a tag that is placed above the metallic surface respectively with a gap height of 0.125" (3.18 mm), 0.25" (6.35 mm), and 0.5" (12.7 mm), as shown in Fig. 2.6. The experiments read an Alien Squiggle RFID tag for 100 trials. The vertical distance between the RFID tag and the reader antenna is 60" (1.52 m) and the horizontal distance is 17" (0.43 m).

For the 0.125" gap case, the RFID reader obtains 0 valid readings, that is, the reader fails to read the tag for all the trials. For the 0.25" gap case, 42 successful RSSI measurements are observed. The average RSSI was 86.85 in this case. For the 0.5" gap case, we obtained 100 successful RSSI measurements, and the average RSSI is 83.89.

While the air gap is not immediately applicable solution for deck operation, the air gap can be replaced with thin and strong dielectric materials, provided that the RFID tag antennas are properly redesigned to match the dielectric material being used.

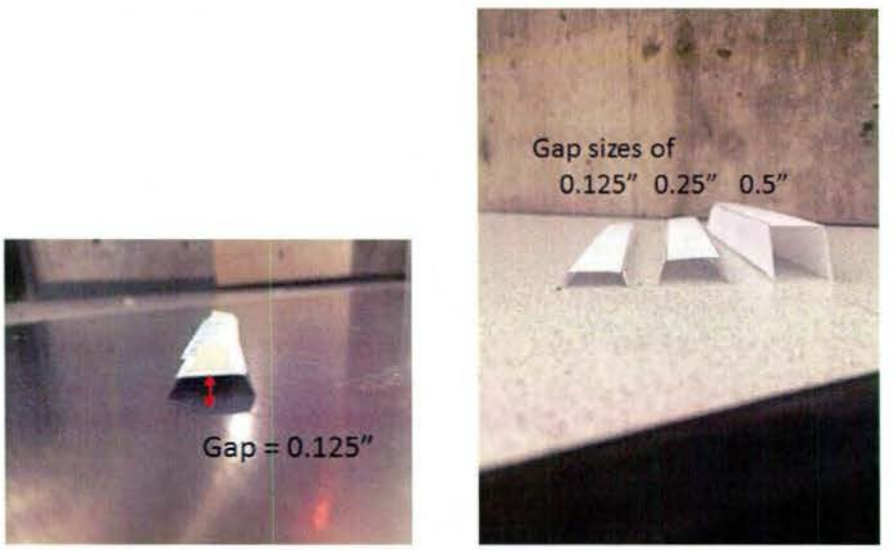

Fig. 2.6. RFID tags placed above metallic surface with different heights of air gaps.

2.3.3. Measured RSSI with Form between Standard Tag and Metallic Sheet

Using form gaps instead of air gaps would be more convenient for experimental evaluation. We tested two types of foams at different gap widths of 0.75", 0.375", 0.25", and 0.125". The first type of foam is the Expanded Polystyrene foam (Styrofoam) which is popularly used as an "electromagnetically invisible" material in antenna experiments. The second one is the Owens Corning Extruded Polystyrene foam (XPS) which was chosen because of its rigid structure. The XPS foam is significantly easier to work with than the Styrofoam for cutting to precise thicknesses.

The experimental scene is shown in Fig. 2.7. All of the measurements are made with a distance of 30" between the antenna and tag, with a 3/8" thick steel plate beneath the tag and foam. Each reported RSSI value was computed from an average of 100 independent reads.

As depicted in Fig. 2.8, the two types of foam performed almost identically at all four distances tested. It appears that any gap between about 0.2" and 0.75" will likely result in an acceptable readability. The XPS foam was chosen as the material for future experiments because it performs as well as the Styrofoam while being easier to work with.

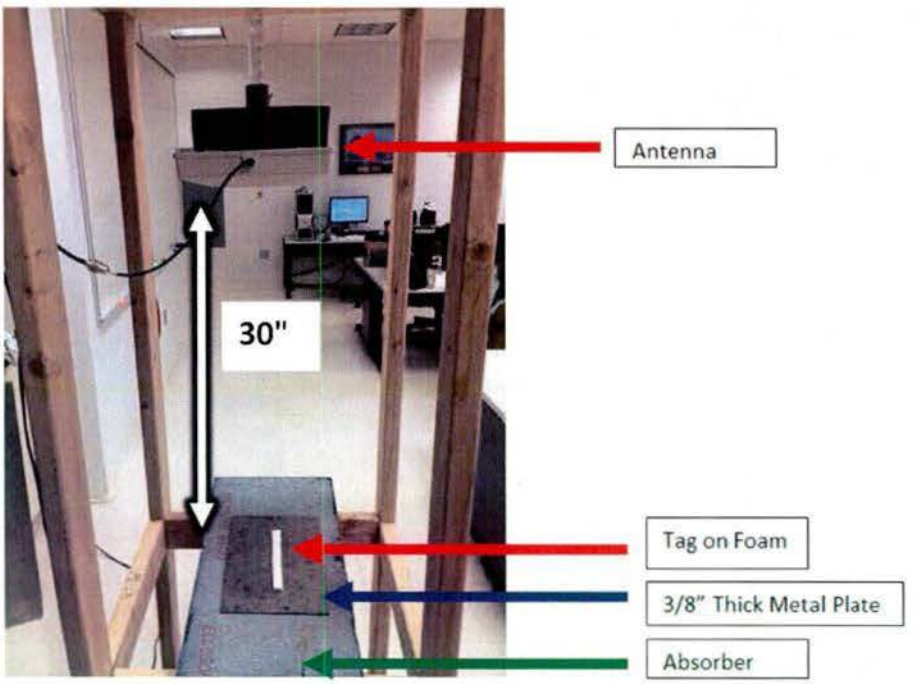

Figure 2.7. Experimental scene.

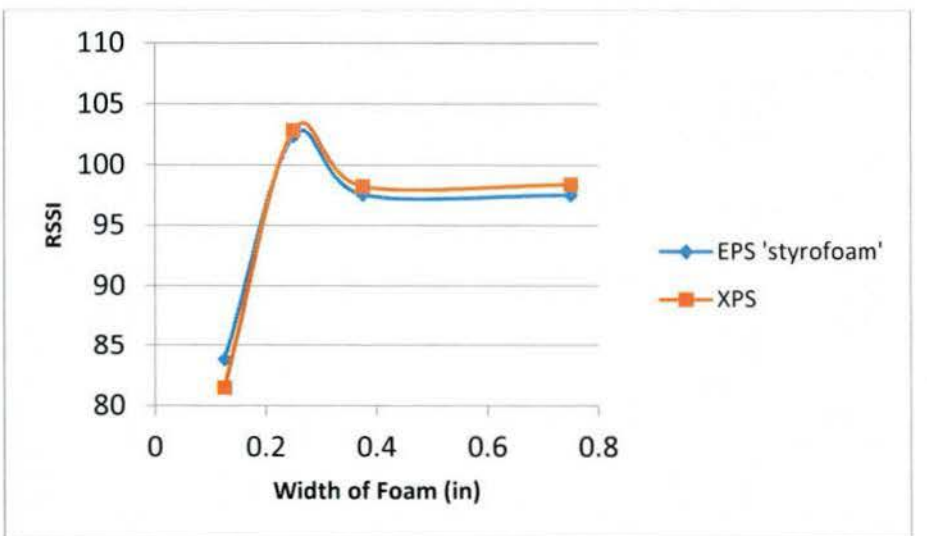

Figure 2.8. Effect of form gap width to the RSSI performance.

2.4. Measured RSSI versus Range

In this section, we report the results of RSSI versus reader-tag range for standard tags that are placed on metallic surface with a form gap, and for Omni-ID Max metal surface tags that are directly placed on a metallic surface. The relationship between RSSI and tag orientation is reported in Section 2.5.

Overall, for both types of tags, the RSSI readings show clear relationships to the reader-tag range and to the tag orientations. Such relationships differ between the two types of tags, and differ to those observed in free space without the metallic surface. Nevertheless, when calibrated references are used, the measured RSSI results can be used for RFID reader localization, as we performed in the free-space situations.

To create the metallic surface environment, we used a 6' x 6' aluminum floor with the wooden RFID test stand. In each experiment the tag was mounted directly below the antenna at a given distance and the RSSI was recorded as the average of 100 measurements. The Omni-ID Max tags were mounted directly to the metallic floor, while the standard tags were placed on the floor with a 0.25" XPS foam gap.

As shown in Fig. 2.9, both the standard tag with foam and the Omni-ID Max tags exhibit reasonably linear relationships between the RSSI and the reader-tag distance. It should be noted that, while the standard tag report a higher RSSI value across the entire range of distances, the reading rate became much slower when the reader-tag distance is larger than 41". To successfully read the standard tags at distances greater than 41", the reading rate has to be reduced to about 1.6 reads/second, compared to the original read rate of 5 reads/second.

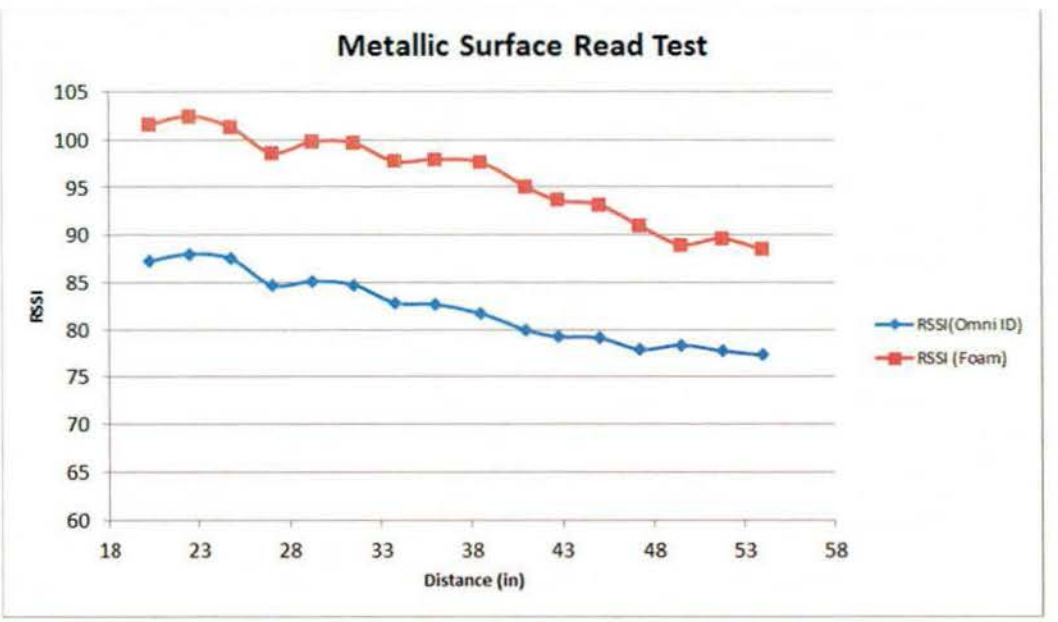

Figure 2.9. RSSI with distance for two types of tags.

2.5. Measured RSSI versus Tag Orientation

2.5.1. RSSI versus Tag Orientation for Standard RFID Tags with Form

To understand the relationship between the RSSI and the angle of the metallic surfaces, we designed an experiment to rotate the tag and the metallic surface beneath the tag to specific angles. The tags were placed on a rotating piece of 0.25" thick aluminum affixed with an angle measure. Measurements were then taken at various rotation angles as described in Fig. 2.10.

The RSSI of a standard tag with 0.25" foam is shown in Fig. 2.11 with respect to the tag orientation, where the metallic surface is kept level. The RSSI shows a small variation in this case.

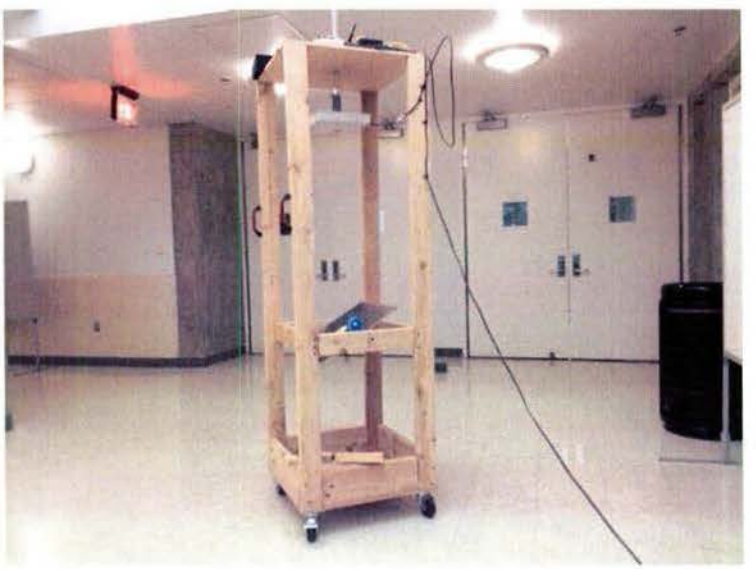

Figure 2.10. Experiment setting for the measurement of RSSI versus angle relationship.

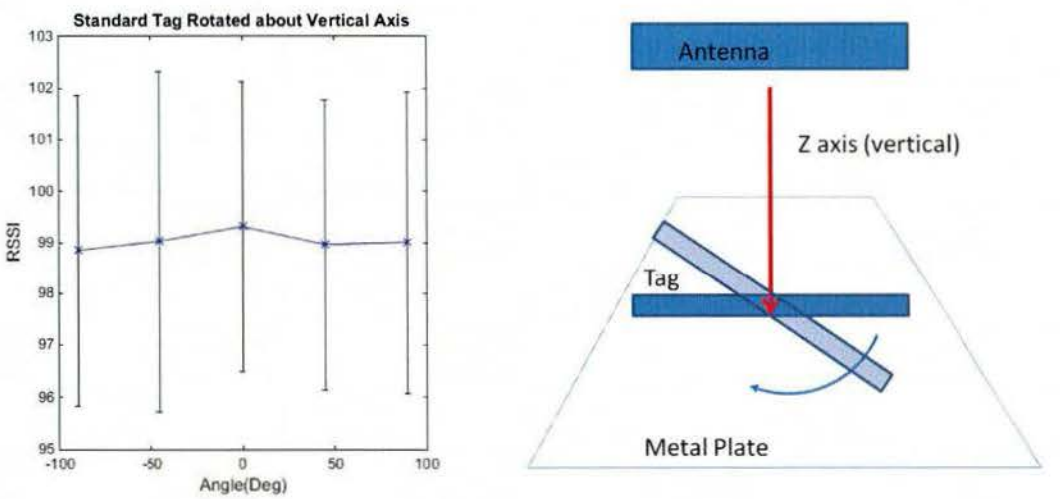

Figure 2.11. RSSI measurement with a standard RFID tag rotating on a flat metallic surface.

Fig. 2.12 shows the RSSI results of the same standard tag with 0.25" thick foam, but the tag is rotated around its long axis, and the metallic surface rotates with the tag. This emulates a situation that the reader signal arrives from a side direction with a grazing angle with respect to the flat metallic surface, and the tag is placed on it with 0.25" form. The RSSI maintains a high RSSI level above 95 when the angle is between -50° and 70°, whereas it decreases rapidly when the angle is out of this region.

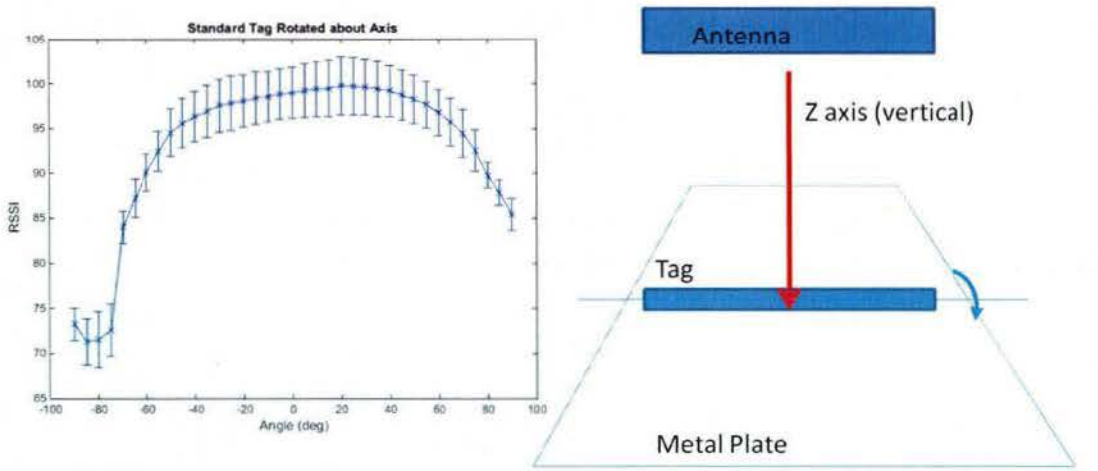

Figure 2.12. RSSI measurement with a standard RFID tag rotating around the tag long-axis with the metallic surface rotating with the tag.

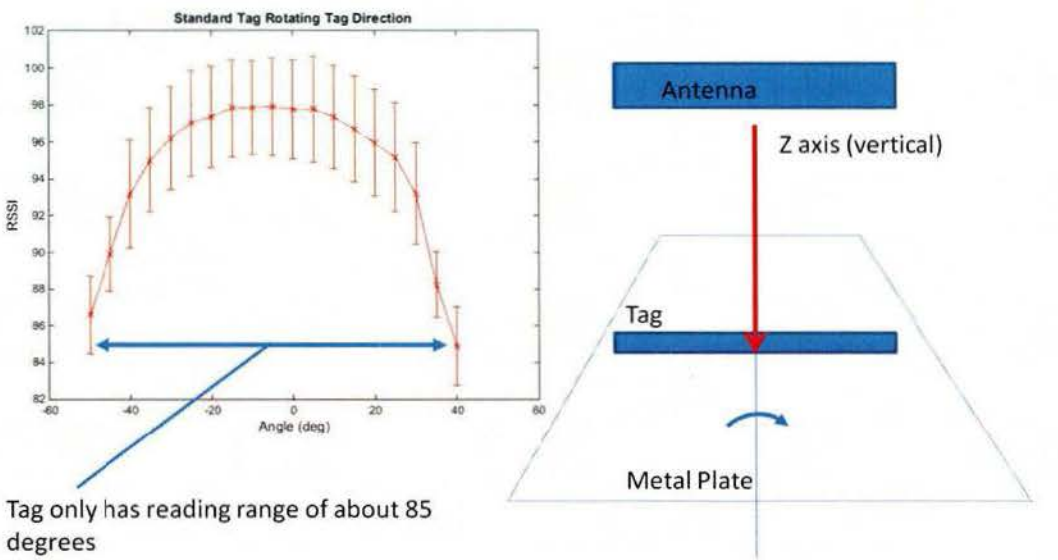

Figure 2.13. RSSI measurement with a standard RFID tag rotating around the tag short-axis with the metallic surface rotating with the tag.

Fig. 2.13 shows the RSSI results of the same standard tag with 0.25" foam, but the tag is rotated around its short axis. The metallic surface rotates with the tag. This emulates a situation that the reader signal is from the tag long-axis direction with a grazing angle with respect to the flat metallic surface. The tag is placed on it with 0.25" form. The RSSI maintains a high level above 95 when the angle is between -35° and 25°, whereas it decreases rapidly when the angle is out of this region. The read range is much narrower in this case as compared to the results depicted in Fig. 2.12.

3.5.2. RSSI versus Tag Orientation for Standard RFID Tags with Form

The RSSI of the Omni-ID Max tag is shown in Fig. 2.14 with respect to the tag orientation, where the metallic surface is kept level. Compared to the standard RFID tag with form gap, the RSSI of the Omni-ID Max tag shows a higher variation.

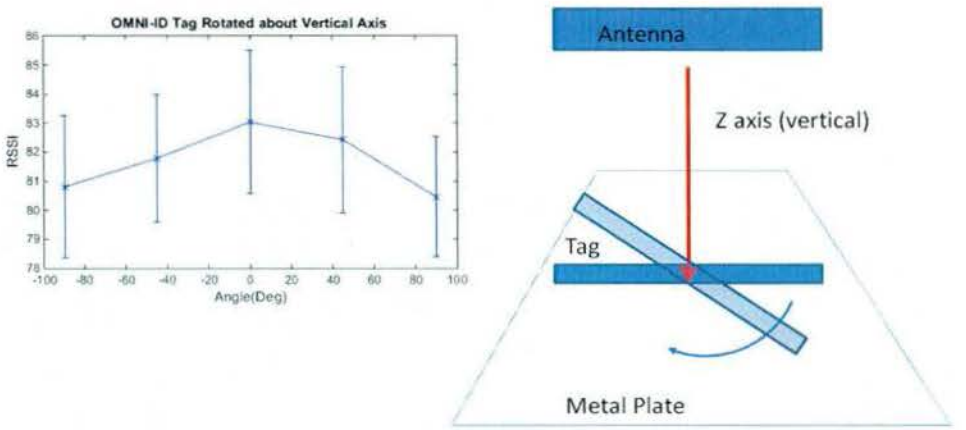

Figure 2.14. RSSI measurement with an Omni-ID Max RFID tag rotating on a flat metallic surface.

Fig. 2.15 shows the RSSI results of the same Omni-ID Max tag when it is rotated around its long axis, and the metallic surface rotates with the tag. As we described earlier, this emulates a situation that the reader signal is from a side direction with a grazing angle with respect to the flat metallic surface, and the tag is placed on it. Compared to the standard tag case, the RSSI shows higher sensitivity to the angle, with high asymmetry.

Fig. 2.16 shows the RSSI results of the same Omni-ID Max tag, but the tag is rotated around its short axis, and the metallic surface rotates with the tag. As we described earlier, this emulates a situation that the reader signal is from the tag long-axis direction with a grazing angle with respect to the flat metallic surface, and the tag is placed on it. It is interesting to note that, when comparing to the standard tags, the RSSI shows an "M"-shape with a broader width.

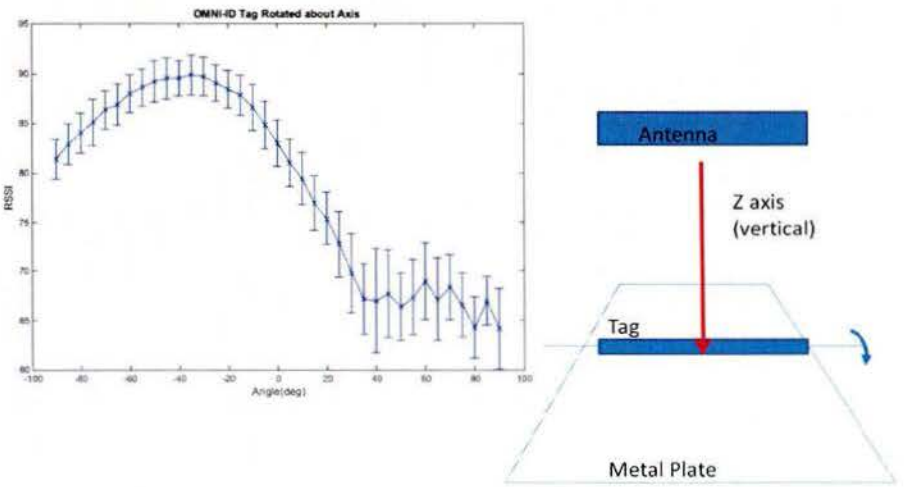

Figure 2.15. RSSI measurement with an Omni-ID Max RFID tag rotating around the tag long-axis with the metallic surface rotating with the tag.

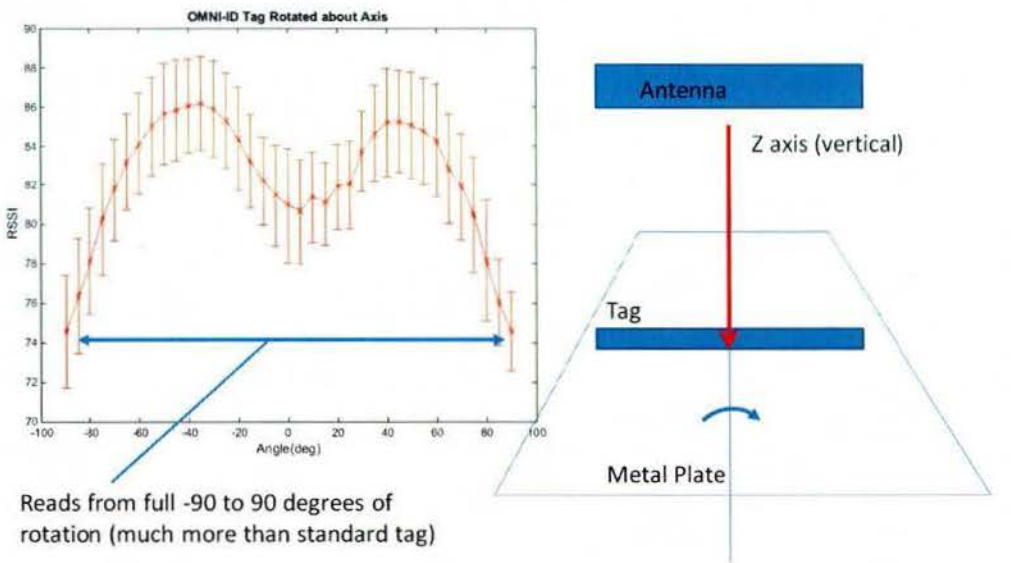

Figure 2.16. RSSI measurement with an Omni-ID Max RFID tag rotating around the tag short-axis with the metallic surface rotating with the tag.

While there are still clear patterns in the RSSI-angle relationships, there is no longer a clear symmetry as we observed in the free space environment, or an approximate symmetry when the standard RFID tags are placed on the metallic surface with a form gap.

2.6. Single-Reader Experimental Results

2.6.1. Experimental Setting

We constructed a tag grid environment for localization and tracking experiments at the side patio of the Villanova University Center for Engineering Education and Research (CEER) building.

To simulate a metallic floor with a low cost, we use aluminum foil beneath the carpet. The carpet function as a uniform gap between the metallic floor and the tags. The total usable area of this tag environment is 24' x 24'.

The tags were placed on a roll of carpet in a "+" formation in an equilateral triangle pattern (separation of 30" between tags). The tag placement is accurate within approximately 1/16". The tags for this test environment were first pre-screened to remove tags outside the desired performance range. All tags selected for the experiment have an RSSI within 0.27% of the mean RSSI at 30".

In the preliminary experiment, the readers were tested on the tag grid to ensure proper functionality. At an RFID reader antenna height of 30", a reader at a given position reads about 21 tags at a time.

The experiments are performed in two different localization scenarios: i) one with the reader moving on a straight path with one instantaneous turn in the middle on a concrete surface, and ii) the other with the reader moving on a constantly winding path on carpet above a smooth metal surface. These two scenarios give examples of an "easy" and "difficult" localization and tracking problem. The non-metallic surface gives better RSSI-based RFID localization results, and the straight paths are more easily predicted by the tracking filter. Inversely, the metallic surface with a curved reader path is more difficult for both localization and tracking. For these two experiments, 50 RSSI measurements per tag were recorded at each position along the path. Additionally on the curved path we repeated the localization and tracking using only 5 RSSI measurements to observe changes in accuracy when only a small amount of RSSI information is available.

2.6.2. Exploitation of Velocity Information

In localization of aircrafts, the velocity information may be estimated from internal measurement. When available, such information can be fused to provide a more accurate tracking performance.

In the following experiments, we provide data for three scenarios for comparison:

- RFID localization only, with no additional state information or tracking;
- Kalman filter tracking using RFID localization estimates;
- Kalman filter tracking using RFID localization estimates and prior knowledge of velocity.

2.6.3. Scenario i: Straight Path

The straight path is shown with results for localization and tracking with no prior velocity information (Fig. 2.17) and for tracking with prior velocity information (Fig. 2.17). The accuracy of the localization and tracking is shown in Table 2.1. It is clear that the Kalman filter tracking is able to improve the accuracy of the position estimate. Compared to using RSSI-based localization

alone, tracking with no prior knowledge of velocity gives a slight improvement to the root mean square error (RMSE) (7% lower) and a significant improvement to minimizing the maximum error (29% lower). Accuracy is further improved when the velocity information is included.

2.6.4. Scenario ii: Curved Path

The curved path with metallic floor represents a very difficult localization scenario. Shown below are localization and tracking results without prior velocity information (Fig. 2.19) and with prior velocity information (Fig. 2.20). The RMSE and the maximum error for the scenario are shown in Table 2.1. While the localization and tracking error is greater than that of the idealized scenario in Figs. 2.17 and 2.18, we achieve a highly accurate localization RMSE of 0.1692 meters (6.661 inches). Kalman filter tracking reduces the RMSE by 5.5% and the maximum error by 27%. The error is further decreased with the inclusion of velocity information in the tracking filter, reducing RMSE by 39% and maximum error by 60%.

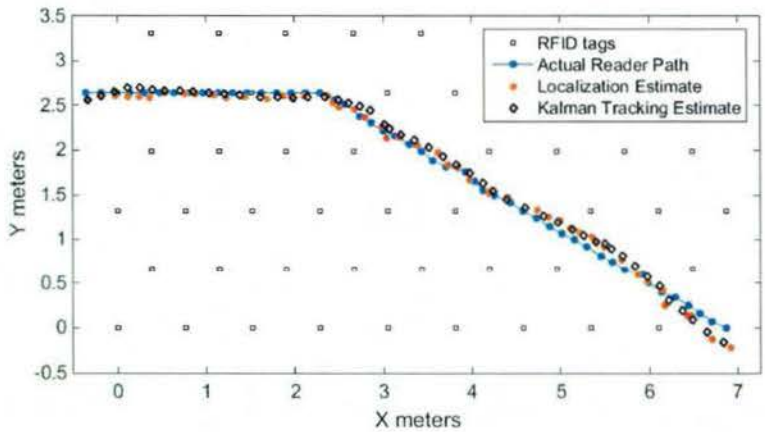

Figure 2.17. RFID localization and tracking, straight path.

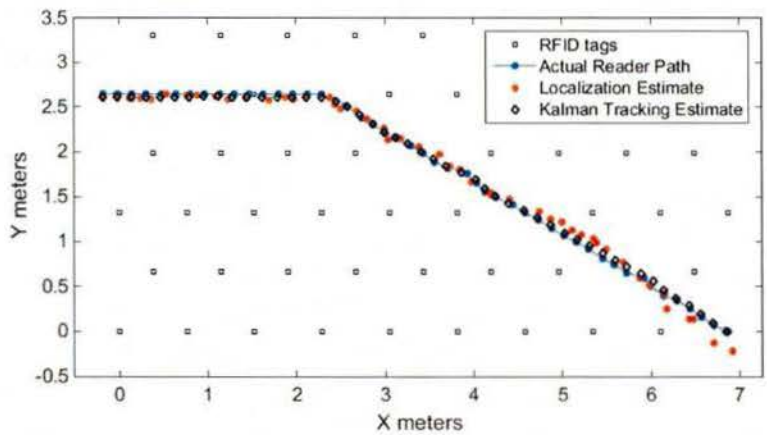

Figure 2.18. RFID localization and tracking with prior velocity information, straight path.

Table 2.1. RMSE and maximum error for localization and tracking experiments

Meters	Straight Path 50 Samples		Curved Path 50 Samples		Curved Path 5 samples	
	RMSE	Max Error	RMSE	Max Error	RMSE	Max Error
Localization	0.108	0.2383	0.1692	0.4123	0.1672	0.4228
Tracking Without Known Velocity	0.1005	0.1701	0.1599	0.2985	0.1636	0.3189
Tracking With Known Velocity	0.0367	0.0662	0.1035	0.1663	0.1004	0.1638

Inches	Straight Path 50 Samples		Curved Path 50 Samples		Curved Path 5 samples	
	RMSE	Max Error	RMSE	Max Error	RMSE	Max Error
Localization	4.25	9.38	6.66	16.23	6.58	16.65
Tracking Without Known Velocity	3.96	6.70	6.30	11.75	6.44	12.56
Tracking With Known Velocity	1.44	2.61	4.07	6.55	3.95	6.45

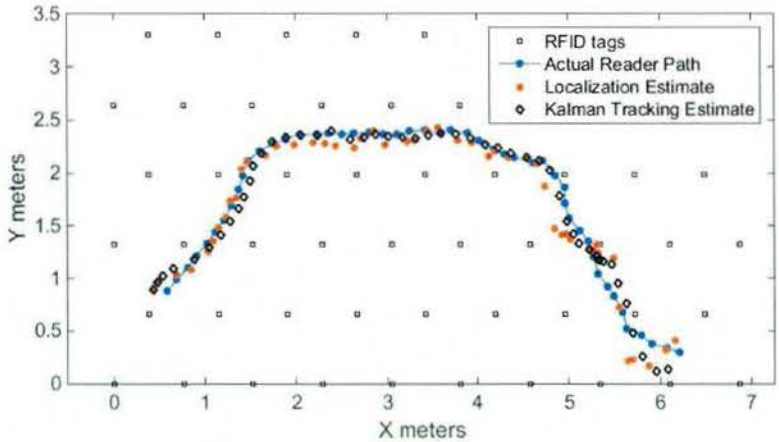

Figure 2.19. RFID localization and tracking, curved path with metallic floor.

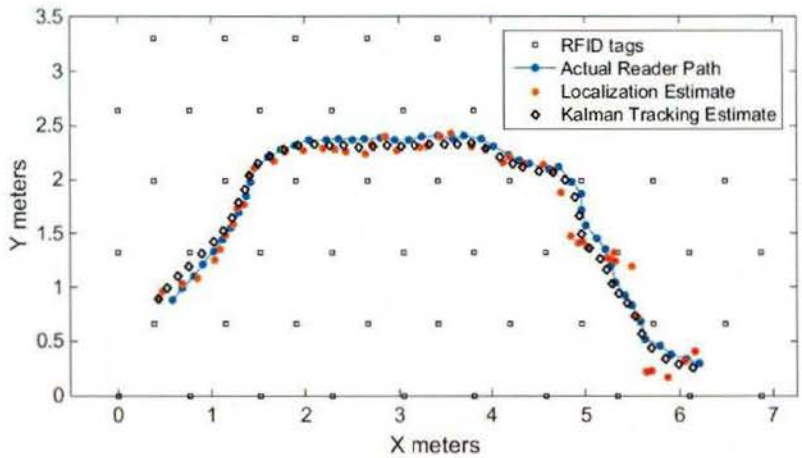

Figure 2.20. RFID localization and tracking with prior velocity information, curved path with metallic floor.

The curved path localization and tracking are implemented again using only 5 RSSI samples rather than 50 to simulate a fast-moving reader that has very little time to collect samples. The

localization and tracking results are shown below in Figs. 2.21 and 2.22 and the error analysis is included in Table 2.1. The accuracy is very similar to the 50 samples experiment, showing that averaging approximately 5 RSSI samples is sufficient to converge to a localization solution.

From the results obtained in these experiments, we conclude that the performance (in terms of RMSE and maximum error) of the RFID localization system can be significantly improved by implementing a tracking filter. Accuracy is further improved by combining the RFID localization information with vehicle velocity.

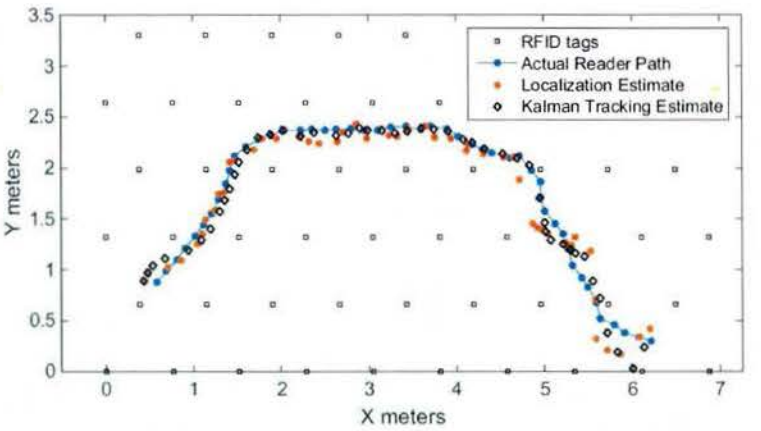

Figure 2.21. RFID localization and tracking, curved path with metallic floor, 5 RSSI Samples

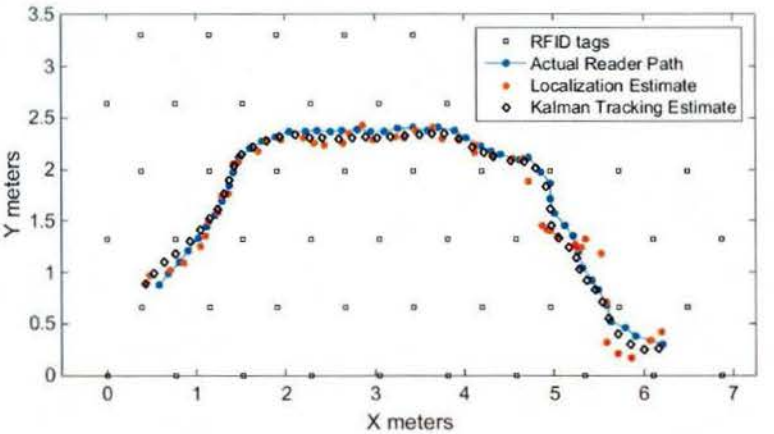

Figure 2.22. RFID localization and tracking with prior velocity information, curved path with metallic floor, 5 RSSI Samples.

2.7. Dual-Reader Experimental Results

In order to uniquely determining the instantaneous location and orientation of an aircraft on deck, at least two RFID readers or RFID reader antennas are required. We have carried out dual-reader

experimental studies, and the results show improved position estimation accuracy and accurate calculation of the orientation angle of the mobile unit to which the readers are attached.

For the dual-reader localization test, two identical RFID readers and antennas were set up on our mobile test stands. These stands were connected together with antennas separated by a distance of 78 inches. Each antenna was positioned 53 inches above the ground. Figure 2.23 shows a sketch of the experiment.

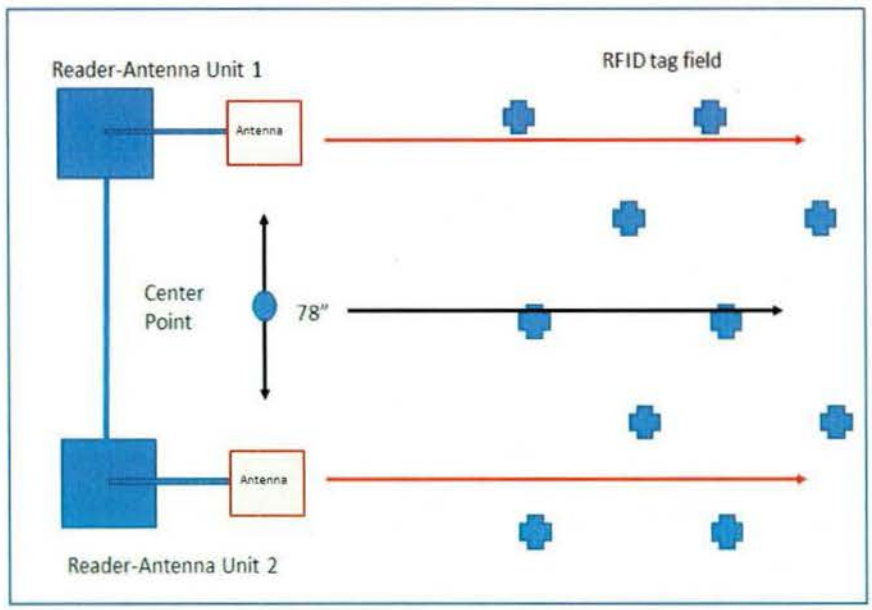

Figure 2.23. Dual-reader experiment setup.

The coupled reader-antenna assembly was pushed through the tag field in a straight line with 50 RSSI measurements per reader taken under a "stop and go" scheme with every 6 inches of travel.

The center point localization is performed by first independently localizing both antennas at each measurement position. At each position, both readers are each assigned position estimates using the ML localization algorithm from our previous work. Denote the estimated positions of the two reader antennas as (x_1, y_1) and (x_2, y_2), respectively. As the center point is physically located directly between the two antennas, its position is estimated by taking the averages of the position estimates for both RFID antennas, i.e., $((x_1+x_2)/2, (y_1+y_2)/2)$. The orientation of the dual-reader assembly is then calculated from $\theta = \tan^{-1}((y_2 - y_1)/(x_2 - x_1))$.

The individual reader antennas are first localized independently as shown in Fig. 2.24. The reader on path 1 has an RMS localization error of 3.1 inches and the reader on path 2 has an RMSE of 3.6 inches. Fig. 2.25 shows the path of the center point and the position and orientation estimates calculated from the averages of the two individual paths. With an RMSE of 2.4 inches, the dual-reader position estimate has improved accuracy over the single-reader estimates.

Fig. 2.26 shows the error of the orientation estimate from the true orientation angle. The orientation angle estimate achieves a high accuracy with an RMSE of 3 degrees and a maximum error of 6 degrees.

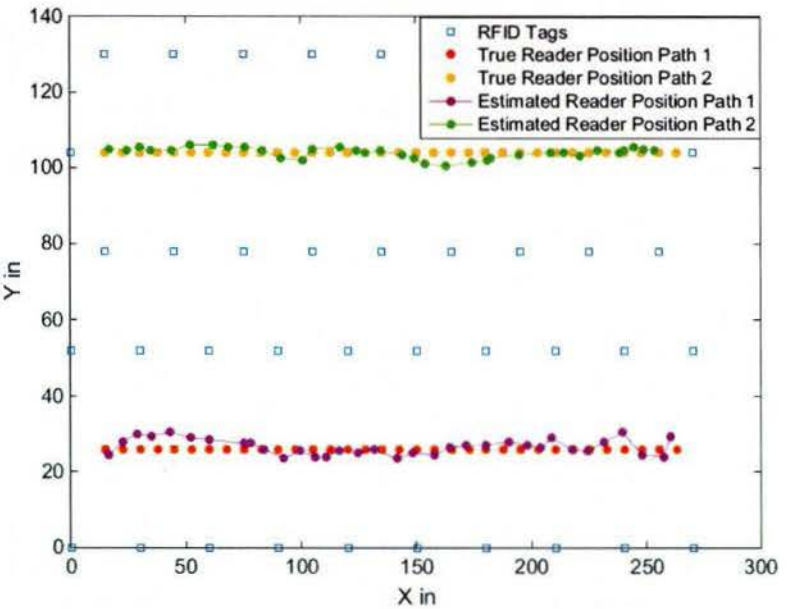

Figure 2.24. True and estimated positions of the two reader antennas.

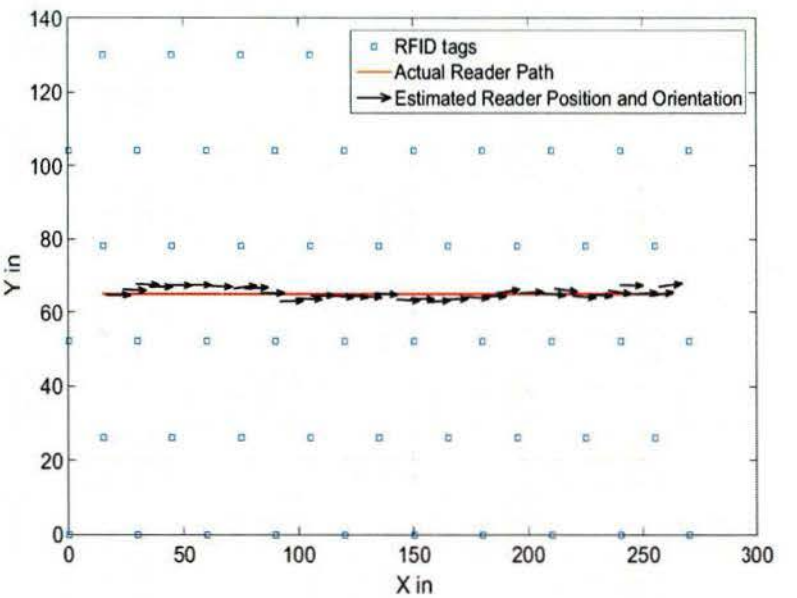

Figure 2.25. Path of the center point of the dual-reader assembly with arrows showing the position and orientation estimate at each point on the path.

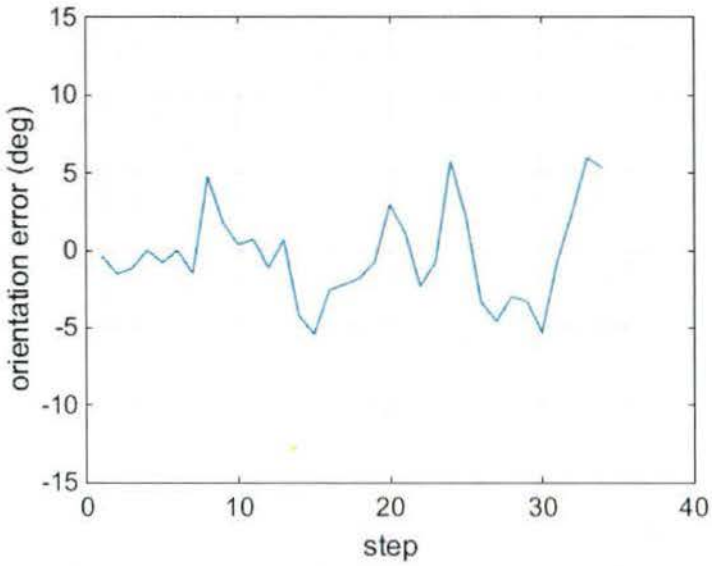

Figure 2.26. Orientation angle error at each step in the reader's path.

3. Region of Interest Identification via Computer Vision

The proposed work under this task is to fuse the computer vision based region of interest (ROI) identification algorithms, developed by the RISE Lab, to the RFID-based localization and tracking system. The RISE Lab has developed a localization and tracking algorithm based on machine vision and camera data acquisition. It uses pure image analysis techniques through object extraction from the deck background with subsequent identification and tracking. This can be used for the identification of ROI of an object located on deck. However, the machine vision algorithms in a maritime environment may suffer from unreliable performance.

It was originally proposed that the vision based ROI identification would enhance the speed at which the RFID system would initialize its interrogation of tags. In the previous phase, it was determined that there is no speed benefit to supplying the RFID system with an initialization estimate. As such, the vision-based approach is used as a redundant tracking tool that helps maintain a rough track of the aircraft in cases the RFID system fails (i.e., areas of destroyed/degraded tags). In addition, the RISE Lab has used both the vision-based and the RFID-based algorithms to determine the "ground truth" in the analysis of the test results.

4. Conclusion

We have developed a promising RFID-based technique for accurate aircraft localization and tracking onboard a carrier. The effectiveness of the proposed technique is verified through experimental results. Under the support of our team, the NAVAIR RISE Lab performed experimental verifications and confirmed the effectiveness of the proposed techniques.

References

[1] D. M. Dobkin, *The RF in RFID: UHF RFID in Practice*. Newnes, 2012.

[2] S. Subedi, Y. D. Zhang, and M. G. Amin, "Precise RFID localization in impaired environment through sparse signal recovery," in *Proceedings of SPIE Defense, Security, and Sensing*, Baltimore, MD, vol. 8753, May 2013.

[3] E. Pauls and Y. D. Zhang, "Experimental studies of high-accuracy RFID localization with channel impairments," in *Proceedings of SPIE Mobile Multimedia/Image Processing, Security, and Applications*, Baltimore, MD, vol. 9497, April 2015.

[4] N. Gordon, B. Ristic, and S. Arulampalam, *Beyond the Kalman Filter: Particle Filters for Tracking Applications*. Artech House, 2004.

[5] D. M. Pozar, *Microwave Engineering, Third Edition*, John Wiley, 2011.

REPORT DOCUMENTATION PAGE

Form Approved
OMB No. 0704-0188

1. REPORT DATE *(DD-MM-YYYY)*	2. REPORT TYPE	3. DATES COVERED *(From - To)*
30-06-2017	Final	01-06-2016 - 31-05-2017

4. TITLE AND SUBTITLE
Localization Grid for Accurate Positioning Onboard a Carrier

5a. CONTRACT NUMBER

5b. GRANT NUMBER
N00014-16-1-2425

5c. PROGRAM ELEMENT NUMBER

6. AUTHOR(S)
Zhang, Yimin D. (PI)

5d. PROJECT NUMBER

5e. TASK NUMBER

5f. WORK UNIT NUMBER

7. PERFORMING ORGANIZATION NAME(S) AND ADDRESS(ES)
Temple University
Philadelphia, PA 19122

8. PERFORMING ORGANIZATION REPORT NUMBER
310316

9. SPONSORING/MONITORING AGENCY NAME(S) AND ADDRESS(ES)
Office of Naval Research
Code 35, Naval Air Warfare & Weapons
875 N. Randolph St.
Arlington, VA 22203

10. SPONSOR/MONITOR'S ACRONYM(S)

11. SPONSOR/MONITOR'S REPORT NUMBER(S)

12. DISTRIBUTION/AVAILABILITY STATEMENT
DISTRIBUTION STATEMENT A. Approved for public release. Distribution is unlimited.

13. SUPPLEMENTARY NOTES

14. ABSTRACT
The objective of this project is to develop implementable solutions that achieve the required instantaneous position and orientation tracking accuracy of aircrafts onboard a deck with the radio frequency identification (RFID) technologies. RFID tags covering the entire flight deck and hanger bay areas serve as anchors with known locations, whereas an aircraft, through multiple RFID reader antennas which are fixed on the aircraft, senses the relative position information with nearby RFID tags and determines its own instantaneous position and orientation. We provide technical supports for the NAVAIR to perform experimental verification to assess the feasibility of the techniques we have developed in this project.

15. SUBJECT TERMS
Aircraft tracking, deck operation, radio frequency identification (RFID)

16. SECURITY CLASSIFICATION OF:			17. LIMITATION OF ABSTRACT	18. NUMBER OF PAGES	19a. NAME OF RESPONSIBLE PERSON
a. REPORT	b. ABSTRACT	c. THIS PAGE			19b. TELEPHONE NUMBER *(Include area code)*
UU	UU	UU	UU	31	